Journal of the Korean Ceramic Society
Vol. 55, No. 4, pp. 392–399, 2018.

https://doi.org/10.4191/kcers.2018.55.4.11

Mechanical Properties of C_f/SiC Composite Using a Combined Process of Chemical Vapor Infiltration and Precursor Infiltration Pyrolysis

Kyung-Mi Kim*,, Yoonsoo Hahn*, Sung-Min Lee*, Kyoon Choi*,† and Jong-Heun Lee****

**Icheon Branch, Korea Institute of Ceramic Engineering and Technology, Icheon 17303, Korea*
***Department of Materials Science and Engineering, Korea University, Seoul 02841, Korea*

(Received May 9, 2018; Revised June 20, 2018; Accepted June 26, 2018)

ABSTRACT

C_f/SiC composites were prepared via a process combining chemical vapor infiltration (CVI) and precursor infiltration pyrolysis (PIP), wherein silicon carbide matrices were infiltrated into 2.5D carbon preforms. The obtained composites exhibited porosities of 20 vol % and achieved strengths of 244 MPa in air at room temperature and 423 MPa at 1300°C under an Ar atmosphere. Carbon fiber pull-out was rarely observed in the fractured surfaces, although intermediate layers of pyrolytic carbon of 150 nm thickness were deposited between the fiber and matrix. Fatigue fracture was observed after 1380 cycles under 45 MPa stress at 1000°C. The fractured samples were analyzed by transmission electron microscopy to observe the distributed phases.

Key words : Ceramic Matrix Composite (CMC), Chemical Vapor Infiltration (CVI), Precursor Infiltration Pyrolysis (PIP), Fatigue, Transmission Electron Microscopy (TEM)

1. Introduction

The ceramic matrix composite (CMC) based on carbon/carbon composite was developed as a lightweight structural material for the aerospace industry in the 1970s.[1-4] Silicon carbide is used as a structural material in high-temperature applications due to its excellent oxidation resistance, thermal shock resistance, and good chemical and mechanical compatibility with carbon.[5-8] The strength and fracture toughness can be further improved by applying silicon carbide to the matrix of the composite.[9-11] Therefore, carbon/silicon carbide composites can be used in engine blades and nozzles in supersonic vehicles which require not only high specific strength but also stability in temperatures as high as 1650°C.[3,4]

CMCs are usually manufactured through one or a combination of the following processes: silicon melt infiltration (SMI), precursor infiltration and pyrolysis (PIP), and chemical vapor infiltration (CVI). In the SMI process, polymer impregnated in the preform is pyrolyzed to create a reactive carbon which in turn reacts with liquid silicon at about 1500°C to form the SiC matrix.[12] The advantages of this process include a short manufacturing time, low cost, and scalability, but some remnant carbon or unreacted silicon can produce C/C-SiC composites. The PIP method produces a silicon carbide matrix through pyrolysis of a polymer precursor containing both silicon and carbon, such as polycarbosilane (PCS).[8,13] This process can produce a matrix containing carbon and silicon carbides of varying composition at relatively low temperatures. However, since the yield of the pyrolysis step is low, the PIP processes has to be repeated several (generally six to ten) times to achieve an acceptable density. In addition, microcracks formed due to inhomogeneous contraction during pyrolysis remain after this repetitive process.

The CVI process proceeds via infiltration of the source gas into the preform and subsequent deposition of gaseous species at the fiber surfaces.[14,15] It is possible to form a homogeneous 3C-SiC phase without pores and inclusions, and therefore the mechanical properties of the composite would be highly desirable for applications in extreme environments. The densification behavior of the resultant composite material is mainly influenced by the process temperature and the flow of the infiltration gas, because the reactive gas flows through open pores in the preform. However, deposition on the surface of the preform usually results in the isolation of inner pores and inhibits uniform densification. In the present study, a thermal gradient system confirmed by a computational fluid dynamics (CFD) simulation was designed to prevent the sealing of the composite surface during the CVI process. The CFD simulation also served to optimize parameters for the densification process. The large pores left between the fiber bundles could be effectively filled by conducting repeated PIP processes after the CVI process. Composite specimens were prepared to obtain specific mechanical properties, which were then evaluated, and the microstructures were characterized to predict the resulting behaviors.

†Corresponding author : Kyoon Choi
E-mail : knchoi@kicet.re.kr
Tel : +82-31-645-1456 Fax : +82-31-645-1493

2. Experimental Procedure

The temperature-gradient chemical vapor infiltration (TG-CVI) system was programmed to impose a vertical temperature gradient of 10°C/mm on the preform, from top to bottom. A CFD simulation using COMSOL6.3a was performed to confirm how the temperature gradient inside the preform was formed. The preform is assumed to have hexagonal fiber packing with isotropic permeability.[16] The precise conditions and hardware used for the simulations have been described previously.[17] The specifications of the carbon preform used in the experiment are shown in Table 1. The carbon fibers were woven into 2.5D needle-punched preforms, and the average fiber volume fraction was about 20 vol %. First, pyrolytic carbon (PyC) was coated on the carbon fibers to help the pull-out of carbon fibers during failure of the composite. A PyC layer of 100 – 150 nm thickness was formed on the carbon fibers by a CVI process using a reaction gas of 10 mol% C_3H_6-diluted hydrogen gas. The PyC deposition conditions were a temperature of 880°C at the bottom of the preform, pressure of 1.33×10^4 Pa, mixture gas flow rate of 4 slm, and total process time of 90 minutes.

The PyC-coated preforms were fixed in the holder as shown in Fig. 1. The chamber was evacuated to below 6.66 Pa with a dry pump, and then the temperature of the bottom of the specimen was set to 1000°C. Methyltrichlorosilane (MTS; 99.9%) and hydrogen (99.999%) were used as source gases and mixed to give a 20 mol% MTS-diluted hydrogen gas which was directed into the chamber. The densification process was carried out at a pressure of 1.33×10^3 Pa for 64 h, in order for the reaction gas to penetrate deeply into the preforms. After the CVI process, PIP using polycarbosilane (PCS, Star PCS, Inc., USA) was performed for further densification. The preform impregnated with the PCS solution under vacuum was cured in an oven at 180°C for 2 h, and then the pyrolysis process was performed under an argon atmosphere at 1500°C to convert the PCS to silicon carbide. This PIP process was repeated several times until no further densification occurred.

A three-point bending test and a high temperature fatigue test were conducted to investigate the mechanical properties of the C_f/SiC composite. The composites were cut into bar-shaped specimens ($3 \times 4 \times 45$ mm^3) following ASTM C 1161 standards.[19] To protect the carbon fibers from oxidation, isothermal CVI was carried out at 1.33×10^3 Pa and 1200°C for 10 h. Bending tests were performed with an ultimate test system (R&B Co., Ltd., Korea) at 1300°C under an Ar atmosphere, and at room temperature in air. The fatigue tests were performed with non-standard small dog-bone test specimens as shown in Fig. 2, using an ultimate

Table 1. Specifications of Carbon Fiber Preform

Carbon fiber	Preform type	Manufacturer	Dimensions in mm
Oxy-PAN, Toray T-700	2.5 D needle-punched	Carbon Nano Fibers Co., Ltd.	71(w) × 95(d) × 10(h)

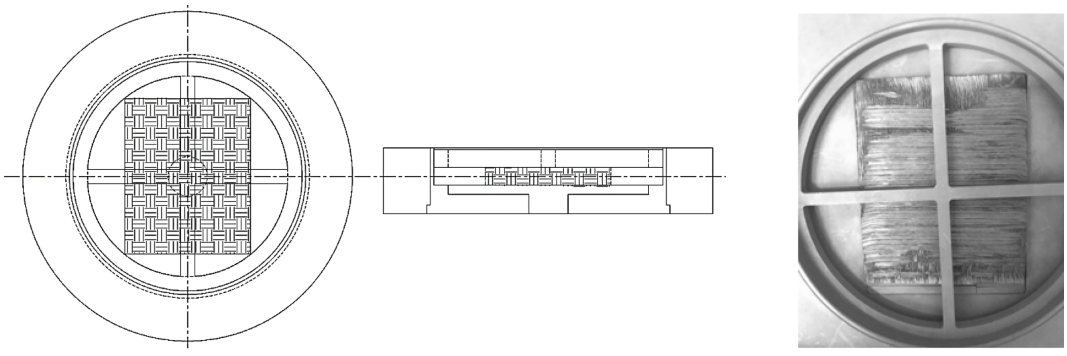

(a) (b)

Fig. 1. (a) CAD diagram and (b) photograph of the holder designed for the CVI experiment.

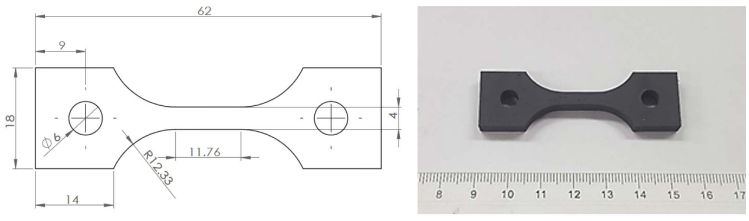

(a) (b)

Fig. 2. (a) Dimensions and (b) photograph of the fatigue specimen.

test system (370 Load Frame, MTS systems Co., Ltd.). Sinusoidal tensile loads of 45 MPa (stress ratio (R) = 0.3, 1 Hz) were applied to the specimen at 1000°C by placing it on 5.8 mm diameter silicon carbide rods (through the holes seen in Fig. 2).

3. Results and Discussions

3.1. Microstructural analysis of the C_f/SiC composite

During the CVI process, silicon carbide began to deposit around the carbon fibers due to surface reactions of the adsorbed species, which resulted in strong binding between fiber and matrix. The cross section of the prepared composite was observed with a scanning electron microscope (JSM-6701F, JEOL Co., Ltd.) as shown in Fig. 3. A homogeneous and dense matrix was created, which is considered to effectively protect the carbon fiber even under an oxidizing atmosphere at high temperature. However, since the large pores between the carbon fiber bundles still remained after the process, it would be inefficient to densify the large pores between the carbon bundles through the CVI process only. The large pores between bundles can be effectively densified through repeated PIP processes. The PIP process is suitable for filling relatively large pores because it forms silicon carbide through the penetration and pyrolysis of the liquid polymer solution. The average apparent density of the composite was 2.17 g/cc and the porosity was estimated to be 20 ± 3%.

The microstructure of the C_f/SiC composite prepared by the combination of CVI and repeated PIP processes is shown in Fig. 4. Most of the large pores between the fiber bundles were reduced, resulting in improved overall densification of the composite. The silicon carbide layer formed by the PIP process was less dense than the layer deposited by the CVI process and exhibited crystal phases with lots of defects such as micro-cracks and voids. These flaws are considered to be due to the thermal stress caused by repeated heat treatment. Therefore, it is believed that the matrix formed by the PIP method does not play a role as a protective layer for preventing oxidation of the fiber at high temperatures. Instead, the dense inner pore-free CVI layers can effectively isolate the carbon fiber from oxidation.

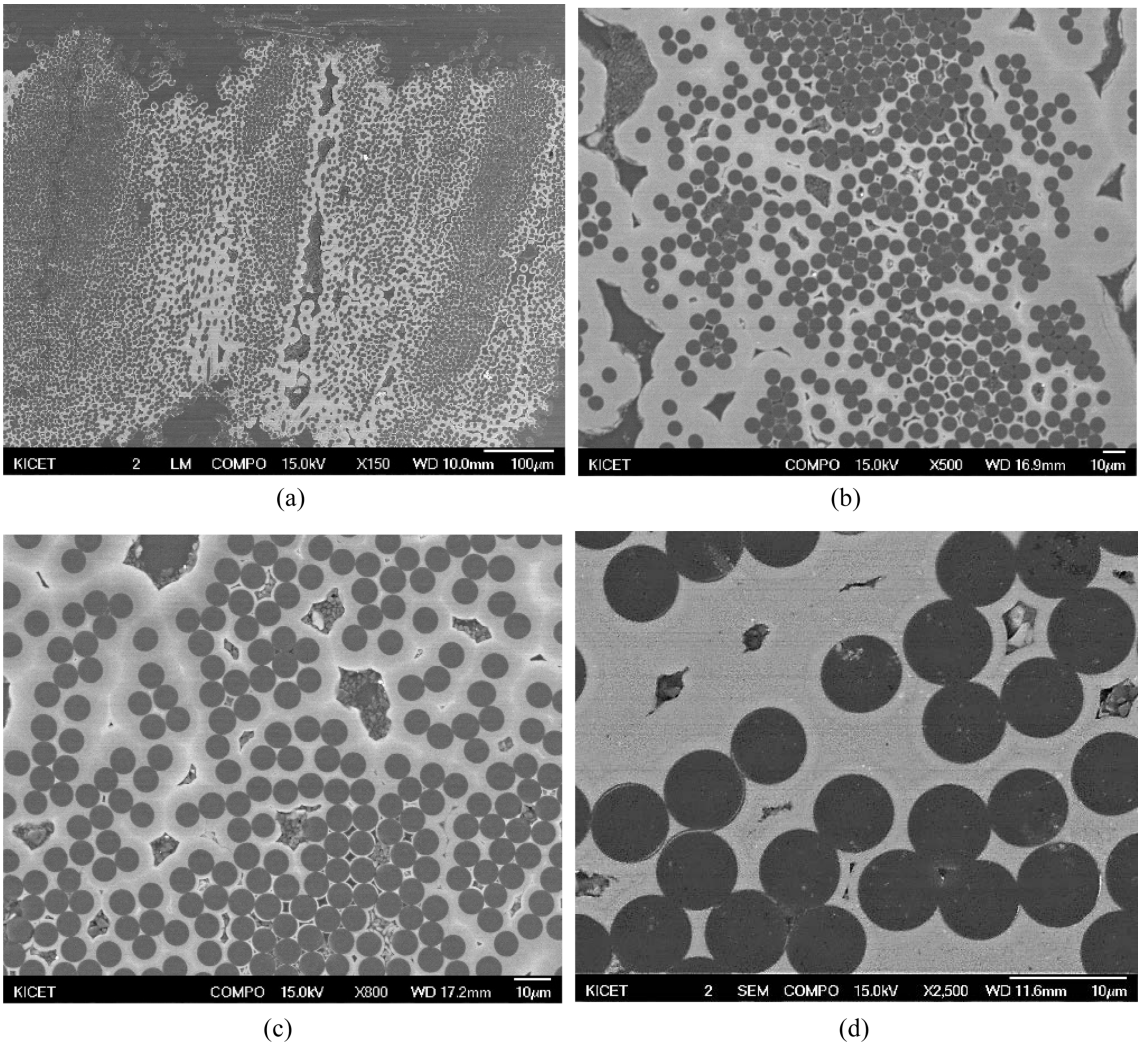

Fig. 3. SEM micrographs of the C_f/SiC composite after the CVI process.

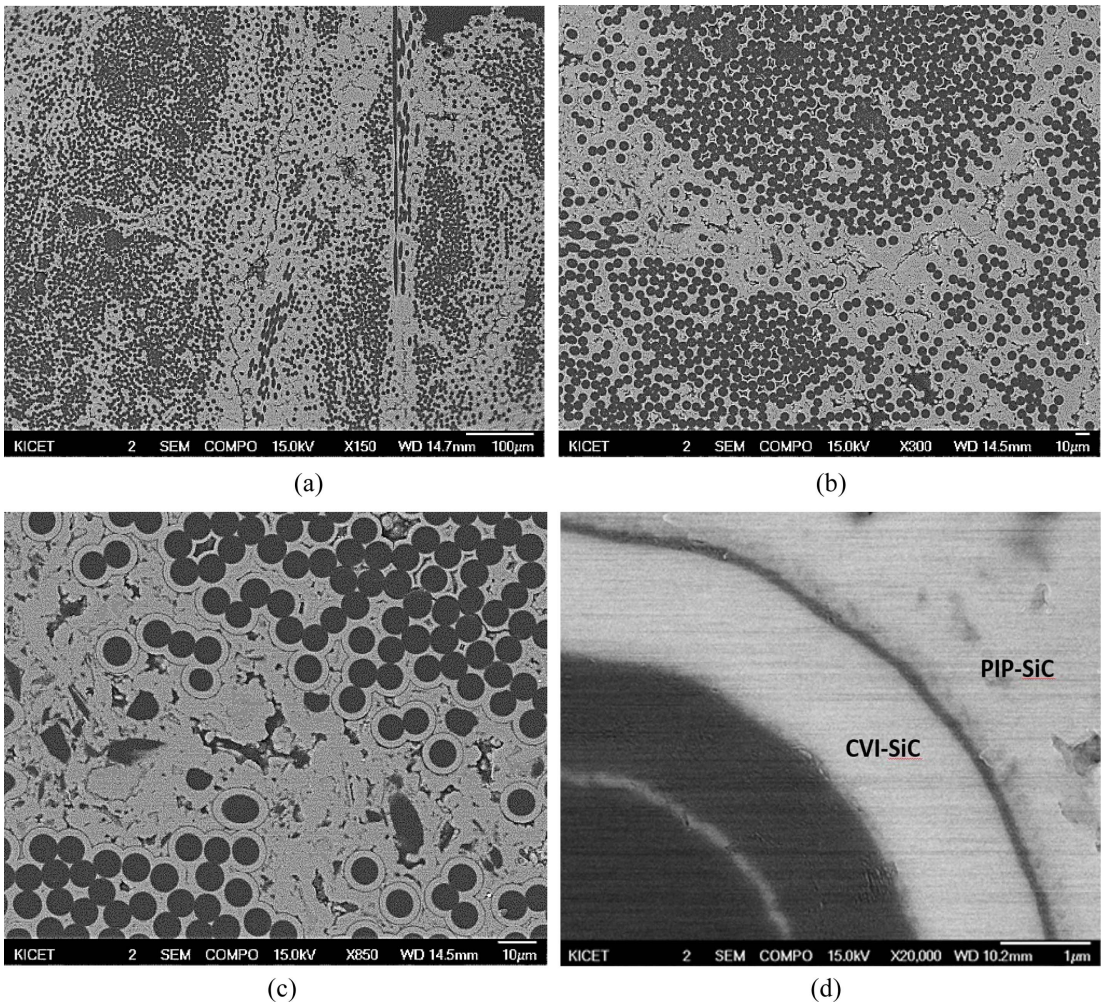

Fig. 4. SEM micrographs of the C_f/SiC composite after the combined process of CVI and PIP.

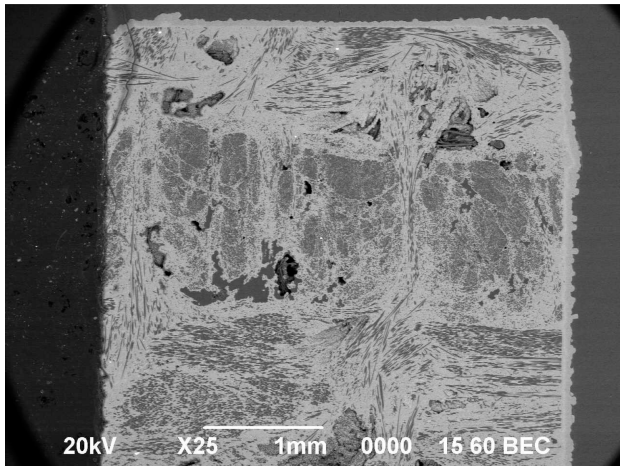

Fig. 5. SEM micrographs of the C_f/SiC composite using a 2.5D carbon preform under low magnification.

The overall shape of the fabricated sample is shown in Fig. 5. The carbon fiber bundles were stacked in alternating 0° and 90° angles, and then the larger fiber bundles were needle-punched to the final preform shape. Some large pores remained in the composite after the combined process of repeated CVI and PIP. Therefore, it was important to reduce the size of the large pores before performing the densification process in order to obtain improved strength and toughness of the composite. It is suggested that the carbon preform should be casted into a carbon mold to squeeze out the air between the bundles, and then the mold can be densified in the CVI system.

3.2. Compositional and structural analysis by transmission electron microscopy

The crystal phases and interfaces of the matrix after completion of the manufacturing process were observed with a transmission electron microscope (Tecnai G2 F30 S-Twin, AP tech Co., Ltd.). TEM specimens were prepared by cutting an area containing both fibers and matrices with a focused ion beam (FIB) system (NOVA 200, FEI Co., Ltd.) as shown in Fig. 6. Fig. 6(a) is a scanning electron microscope (SEM) image of the specimen after the bending test at room temperature. The black rectangular region was cut

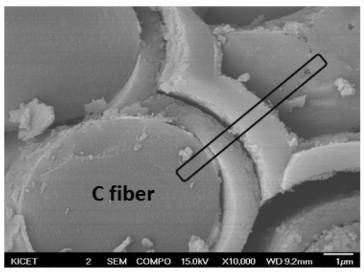

(a)

Area	Carbon	Oxygen	Silicon
A	98.61	0.30	1.08
B	41.50	2.74	55.75
C	96.64	0.62	2.73
D	38.22	1.02	60.75

(b)

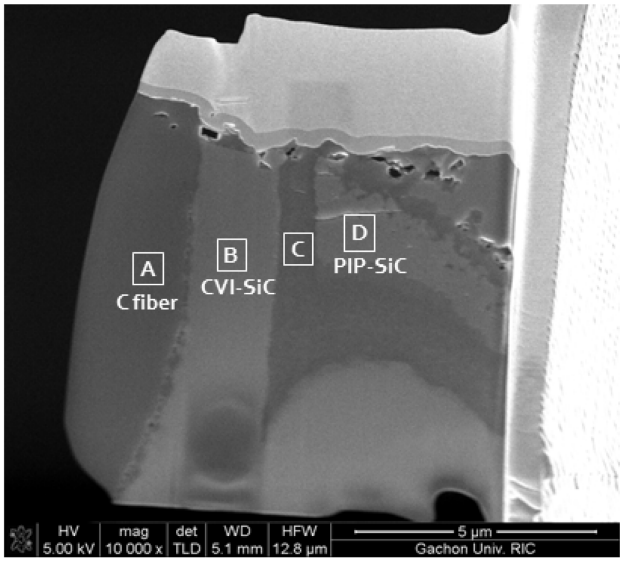

(c)

Fig. 6. (a) Specimen preparation using a FIB for TEM analysis, (b) compositional variations from A to D determined by EDS, and (c) positions of points A to D used for the compositional analysis.

into a slice specimen for TEM analysis. The result of energy-dispersive spectroscopy (EDS) analysis (Fig. 6(b)) reveals the compositions of positions A, B, C, and D as marked on the TEM specimen (Fig. 6(c)). The CVI experiment often resulted in a carbon phase as shown at position C on the TEM specimen, due to accidental lower-temperature processing.

The phase of each position was confirmed through the selected area electron diffraction (SAED) patterns as shown in Fig. 7. The A region is the amorphous layer of a typical turbostratic carbon structure, representing a typical pattern of poly(acrylonitrile) (PAN)-derived carbon fibers.[18]

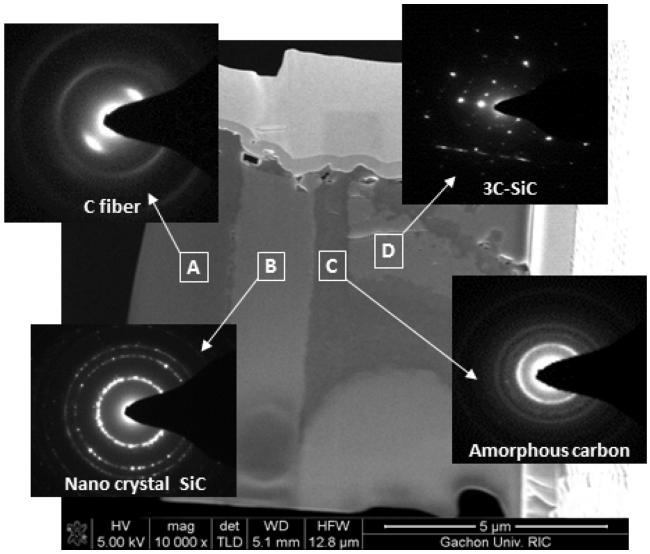

Fig. 7. Selected area electron diffraction (SAED) patterns for regions A–D of the C/SiC composite.

The ring pattern of nanocrystals appears in the B region and is identified as a layer of silicon carbide nanocrystals. On the other hand, only amorphous carbon was recognized in the C region, wherein amorphous carbon was deposited during the CVI process due to the low deposition temperature. Polycrystalline silicon carbide was observed in the D region, which reflected the highly crystalline 3C-SiC phase that was created during the heat treatment within the PIP process.

The carbon layer in the C region observed between the two silicon carbide layers was presumably formed due to the low temperature or excess MTS during the CVI process. At the interface between the fibers in the A region and the matrix in the B region, the PyC layer of approximately 145 nm thickness existed as an amorphous carbon layer as shown in Figs. 8(a) and 8(b). As seen in Figs. 8(c) and 8(d), it is believed that the layer consisting of tens of nanometers of 3C-SiC grains was manufactured by the CVI process; Fig. 8(d) is a local high-magnification micrograph of Fig. 8(c). The CVI process is carried out at temperatures as low as 900°C, unlike the conventional silicon carbide coating process, and thus the nucleation rate of 3C-SiC crystals is much higher than the growth rate. On the other hand, as shown in Figs. 8(e) and 8(f), the silicon carbide layer in the D region was found outside the amorphous carbon layer in sub-micron size. The D region exhibited lots of microcracks, as observed in Fig. 8(e), and therefore the silicon carbide layer could be produced during the PIP process wherein shrinkage during heat treatment of the precursor induced the microcracks.

3.3. Evaluation of mechanical properties of the C_f/SiC composite

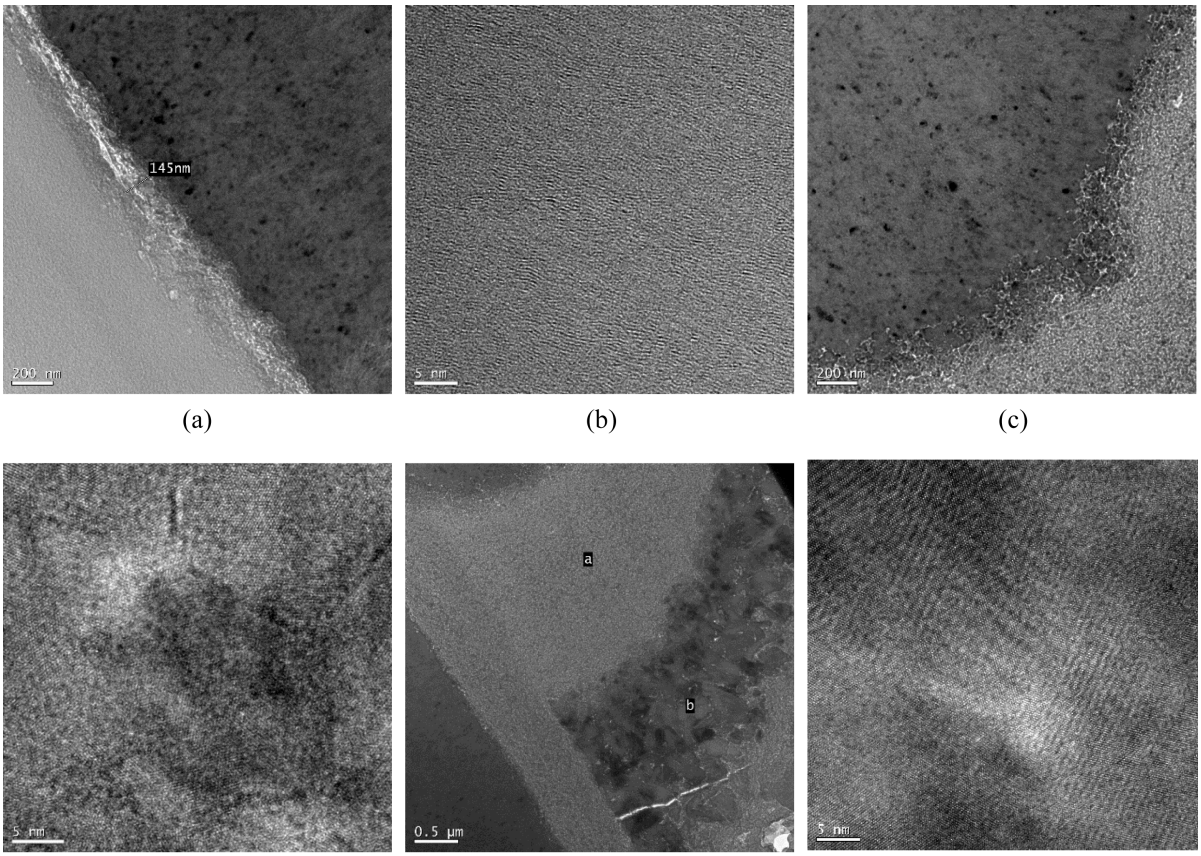

Fig. 8. TEM micrographs of (a, b) PyC, silicon carbide layer grown by (b,c) the CVI , and (e, f) the PIP processes where (b), (d), (f) are local magnifications of (a), (c), (e), respectively.

Fatigue properties were evaluated using the dog-bone-shaped specimens with length of 62 mm and width of 18 mm as shown in Fig. 2. Before the cyclic testing, the ultimate tensile strength (UTS) and proportional limit strength (PLS) in air were estimated to be 270 MPa and 90 MPa, respectively. The tensile-tensile loading was used at 50% of the PLS at 1000°C. The fatigue test was evaluated under the sinusoidal load with a stress ratio (R) of 0.3 and a fre-

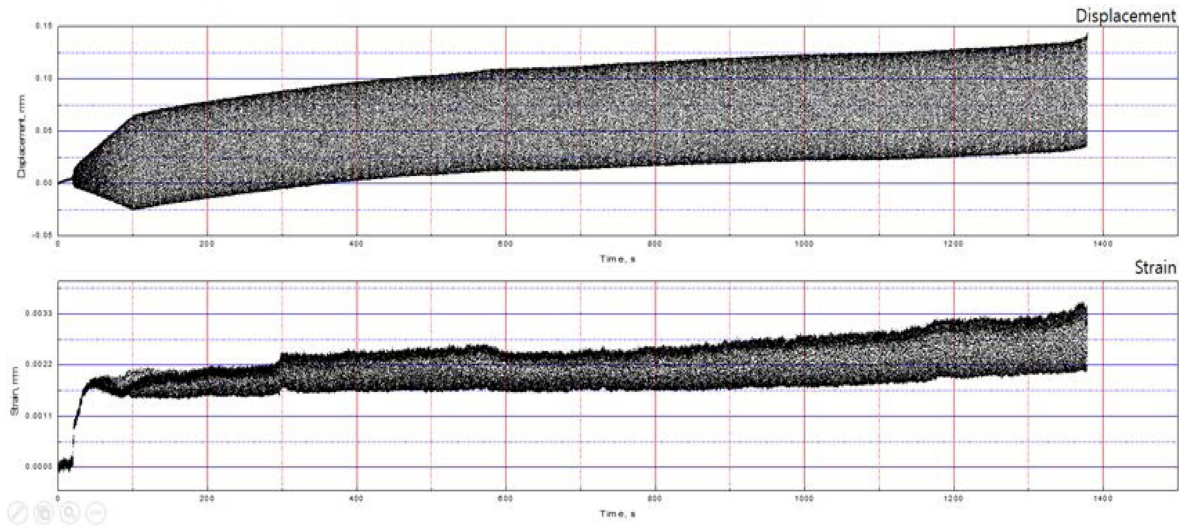

Fig. 9. Results of the fatigue test at 1000°C for the dog-bone specimens which were loaded under 45 MPa with a sinusoidal load with stress ratio (R) of 0.3 and a frequency of 1 Hz.

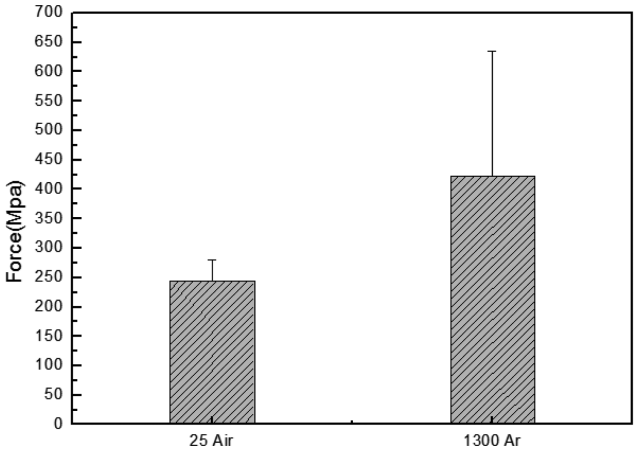

Fig. 10. Strength of C/SiC specimens subjected to a 3-point bending test at room temperature in air and at 1300°C under Ar.

quency of 1 Hz. The hysteresis curves with test numbers to the final failure are shown in Fig. 9. The tensile-tensile fatigue test was stopped upon failure of the specimen after 1380 cycles. Failure would be accelerated by the oxidation of carbon fibers due to penetration of air into the cracks generated and grown during the cyclic test.

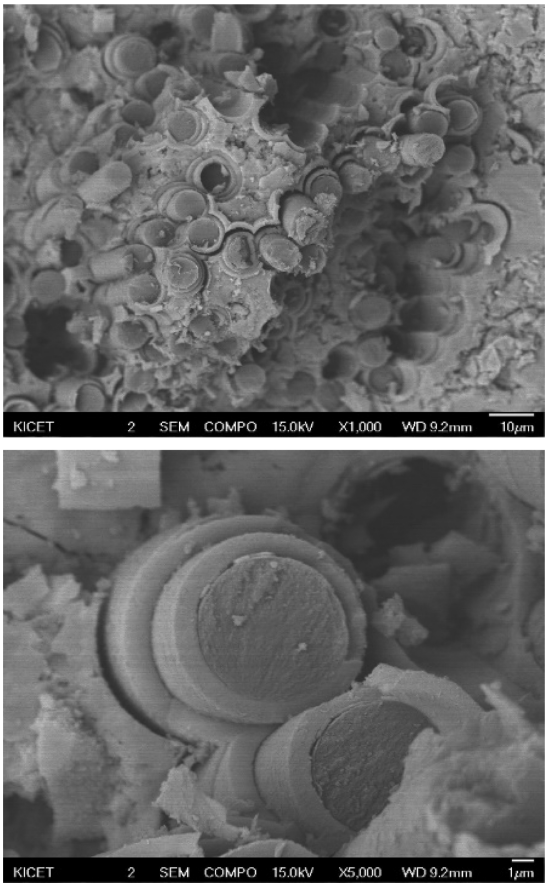

Fig. 11. Fracture surface of the C_f/SiC specimen after being subjected to a 3-point bending test at room temperature.

The 3-point bending tests were done using standard bar-shaped specimens with thickness of 3 mm, width of 4 mm, and length of 45 mm. The strengths at room temperature in air and at 1300°C under an argon atmosphere were 244 MPa and 423 MPa, respectively, as shown in Fig. 10. The standard deviations estimated across 4 samples at room temperature and 7 samples at 1300°C show large variation in the strength values, especially for HT specimens, which reflects the density variations arising due to the CVI process. Large pores, up to a few hundred micrometers, were found (Fig. 5) in the central region of the specimen which might be related to the isolation of this space during the CVI process. The strength at high temperature was notably higher than that at room temperature, which has not been properly explained or understood so far but is thought to be partly due to protection of the carbon fibers by the silicon carbide layers. Further, it was observed that the carbon fibers were pulled out from the silicon carbide matrix in the fractured surfaces of the tested specimen, as shown in Fig. 11. It is believed that the PyC interfacial layer suppresses the propagation of cracks in the direction of maximum stress and relieves the stress through pull-out of the carbon fibers.

4. Conclusions

Oxidation of carbon fibers at high temperatures above 1000°C greatly limits the range of application of silicon carbide composites. In particular, fatigue behavior over long periods of time and at low loads is an important factor in determining the direction of future research, since this is a matter of great concern in the production of materials requiring high reliability such as aircraft parts. One alternative is to apply silicon carbide fibers to composites,[20,21] although there are a limited number of companies that manufacture silicon carbide fibers for high-temperature applications. Therefore, it is currently difficult to procure sufficient quantities of silicon carbide fibers, due to considerations of both time and cost, but this is expected to be resolved in the near future. The method proposed in this study can be extended to silicon carbide/silicon carbide composites, and it is expected that its utilization can lead to improved efficiency in the production of more refined composites.

Acknowledgments

This work was supported by the Ceramic Strategic Research Program, through the Korea Institute of Ceramic Engineering & Technology (KICET). This research was also supported by the Materials/Components Technology Development Program through the Korea Evaluation Institute of Industrial Technology (KEIT) funded by the Ministry of Trade, Industry, and Energy (MOTIE) (grant code: 10065691).

REFERENCES

1. A. G. Evans, "Perspective on the Development of High Toughness Ceramics," *J. Am. Ceram. Soc.*, **73** [2] 187-206 (1990).
2. H. H. Moeller, W. G. Long, A. J. Caputo, and R. A. Lowden, "Fiber-Reinforced Ceramic Composites," *Ceram. Eng. Sci. Proc.*, **8** [7,8] 977-84 (1987).
3. W. J. Sherwood, "CMCs Come Down to Earth," *Am. Ceram. Soc. Bull.*, **82** [8] 25-7 (2003).
4. R. R. Naslain, "SiC-Matrix Composites: Nonbrittle Ceramics for Thermo-Structural Application," *Int. J. Appl. Ceram. Technol.*, **2** [2] 75-84 (2005).
5. J. Wang, L. Zhang, Q. Zeng, G. L. Vignoles, and A. Guette, "Theoretical Investigation for the Active-to-Passive Transition in the Oxidation of Silicon Carbide," *J. Am. Ceram. Soc.*, **91** [5] 1665-73 (2008).
6. J. Meinhardt, T. Woyke, F. Raether, and A. Kienzle, "Measurement and Simulation of the Oxidation of Carbon Fibers and C/SiC Ceramic," *Adv. Sci. Technol.*, **45** [1] 1489-94 (2006).
7. R. Naslain, A. Guette, F. Rebillat, S. Le Gallet, F. Lamouroux, L. Filipuzzi, and C. Louchet, "Oxidation Mechanisms and Kinetics of SiC-Matrix Composites and their Constituents," *J. Mater. Sci.*, **39** [24] 7303-16 (2004).
8. S. Schmidt, S. Beyer, H. Knabe, H. Immich, R. Meistring, and A. Gessler, "Advanced Ceramic Matrix Composite Materials for Current and Future Propulsion Technology Applications," *Acta Astronaut.*, **55** [3] 409-20 (2004).
9. D. B. Marshall and A. G. Evans, "The Mechanical Behavior of Ceramic Matrix Composites," *Acta Metall. Mater*, **37** [10] 2567-83 (1989).
10. A. G. Evans, F. W. Zok, and J. B. Davis, "The Role of Interfaces in Fiber-Reinforced Brittle Matrix Composites," *Compos. Sci. Technol.*, **42** [1-3] 3-24 (1991).
11. J. J. Brennan, S. R. Nutt, and E. Y. Sun, "Interfacial Microstructure and Chemistry of SiC/BN Dual-Coated Nicalon-Fiber-Reinforced Glass-Ceramic Matrix Composites," *J. Am. Ceram. Soc.*, **77** [5] 1329-39 (1994).
12. S. Casadio, A. Donato, and C. A. Nannetti, "Liquid Infiltration and Pyrolysis of SiC Matrix Composite Materials," *Ceram. Trans.*, **58** 193-98 (1995).
13. Y. Katoh, A. Kohyama, S.-M. Dong, T. Hinoki, and J.-J. Kai, "Microstructure and Properties of Liquid Phase Sintered SiC/SiC Composites," *Ceram. Trans.*, **144** 363370 (2002).
14. D. P. Stinton, A. J. Caputo, and R. A. Lowden, "Synthesis of Fibre-Reinforced SiC Composites by Chemical Vapor Infiltration," *Am. Ceram. Soc. Bull.*, **65** [2] 347-50 (1986).
15. A. J. Caputo and W. J. Lackey, "Fabrication of Fiber-Reinforced Ceramic Composites by Chemical Vapor Infiltration," *Ceram. Eng. Sci. Proc.*, **5** [7,8] 654-57 (1984).
16. B. R. Gebart, "Permeability of Unidirectional Reinforcements for RTM," *J. Compos. Mater.*, **26** [8] (1992).
17. K.-M. Kim, J.-W. Seo, K. Choi, and J.-H. Lee, "Improvement of Densification Uniformity of Carbon/Silicon Carbide Composites during Chemical Vapor Infiltration," *Int. J. Nanotechnol., in press.*
18. H. T. Liu, L. W. Yang, S. Han, H. F. Cheng, W. G. Mao, and J. M. Molina-Aldareguia, "Interface Controlled Micro- and Macro-Mechanical Properties of Aluminosilicate Fiber Reinforced SiC Matrix Composites," *J. Eur. Ceram. Soc.*, **37** [3] 883-90 (2017).
19. A. Septiadi, P. Fitriani, A. S. Sharma, and D.-H. Yoon, "Low Pressure Joining of SiC_f/SiC Composites Using Ti_3AlC_2 or Ti_3SiC_2 MAX Phase Tape," *J. Korean Ceram. Soc.*, **54** [4] 340-48 (2017).
20. R. Usukawa, H. Oda, and T. Ishikawa, "Conversion Process of Amorphous Si-Al-C-O Fiber into Nearly Stoichiometric SiC Polycrystalline Fiber," *J. Korean Ceram. Soc.*, **53** [6] 610-14 (2016).
21. T. Ishikawa and H. Oda, "Structural Control Aiming for High-Performance SiC Polycrystalline Fiber," *J. Korean Ceram. Soc.*, **53** [6] 615-21 (2016).